Finite Element Simulation and Experimental Analysis of the Thermo-Mechanical Properties of Dissimilar S275 and 316L Austenite Stainless Steels using the RFW Process

Francois Bayock Njock
Department of Mechanical Engineering, ENSET Douala, University of Douala, Douala, Cameroon
njockfm1@outlook.com (corresponding author)

Martins Kesse
Mechanical Engineering Department, Kwame Nkrumah University of Science and Technology, Ghana
martin.kesse@knust.edu.gh

Maxime Yebga
Department of Mechanical Engineering, ENSET Douala, University of Douala, Douala, Cameroon
maximeyebga@gmail.com

Eric Ndjem Eyike
Department of Mechanical Engineering, ENSET Douala, University of Douala, Douala, Cameroon
eyikecastil1988@gmail.com

Ruben Nlend
Department of Mechanical Engineering, ENSET Douala, University of Douala, Douala, Cameroon
nlendbiss@gmail.com

Received: 18 August 2024 | Revised: 16 September 2024 | Accepted: 4 October 2024

 DOI: https://doi.org/10.48084/etasr.8766

ABSTRACT

This research examines the effect of thermomechanical and microstructural constituents on welding of AISI 316L (austenite stainless steel) and S275 steel. A Finite Element Model (FEM) was constructed using ANSYS 19.1, and an experimental study was conducted using the Rotary Friction Welding (RFW) process. It was determined that there is a genuine correlation between the simulation FEM and the experimental procedure with regard to the thermal profile and ultimate yield strength, particularly when a welding speed of 2,000 rev/min is employed. At that speed, the higher temperature recorded and calculated was 1,450 °C. The discrepancy between the numerical FEM and the experimental temperature profile for the peak temperature calculation was determined to be 2.78%. The mechanical analysis was conducted through tensile force calculations and experiments, the results of which indicated an estimated error of 12%. The calculated error for the ultimate yield strength of the various samples is less than 6% for tensile strength. Upon tensile testing, failure occurred in the S275 sample. The microstructure exhibited increases in Cr and Ni of 1.2% and 1.01%, respectively, in comparison to the base metal of 316L stainless steel.

Keywords-Rotary Friction Welding (RFW); dissimilar metal welding; austenitic stainless steel; S275 structural steel

I. INTRODUCTION

The necessity for the combination of disparate metals arises from the intricate functionality of numerous contemporary industrial applications [1-3]. As manufacturers in a variety of industries prioritize reducing production and operational costs, enhancing mechanical and thermal properties, and providing lightweight solutions for sectors such as shipping, aviation, and automobiles, the use of multiple material combinations for many products is becoming increasingly prevalent [1, 4]. In the

nascent field of joining dissimilar metals for transportation, multi-material solutions comprising steel, aluminum, magnesium, and composites are being employed to supplant monolithic steel structures, thereby reducing not only the weight of vehicles but also enhancing fuel economy [5-10]. The welding of common austenitic stainless steels, such as 304 and 316L, to one another is a routine and relatively straightforward process within the field of fusion welding. Nevertheless, there are numerous instances where it is imperative to weld stainless steel to structural mild steel. There are notable differences in the physical properties of the metals in question, including thermal conductivity and expansion, magnetic properties, metallurgical structure, and corrosion resistance. These differences require careful consideration and attention to ensure optimal results [2, 11-14]. The preceding study demonstrated that welding dissimilar carbon steel and austenite stainless steel by fusion such as Gas Metal Arc Welding (GMAW), resulted in a notable alteration in microstructural composition along the fusion line. Additionally, a corresponding mechanical degradation of properties is observed along the fusion line of the weld. This degradation is attributed to the formation of local high stresses, which are associated with a thermal expansion mismatch between carbon steel and stainless steel [3, 14-17]. This phenomenon has been reported as the primary cause of failure in joints comprising austenitic stainless steel and low-carbon ferrite steel [18-21].

The degradation of mechanical properties that occurs in the fusion zone renders this region a stress raiser, creating a susceptibility to crack propagation and fatigue failure of the welded joints [22-25]. Furthermore, welding a dissimilar stainless steel with carbon steel presents a significant challenge due to the considerable disparity in their thermal conductivity and thermal expansion. This discrepancy can be attributed to the heterogeneous microstructure observed in the weld metal zone [26-34]. A variety of techniques and devices can be employed to assess the cooling rate, mechanical properties, and microstructural constituents within the Heat Affected Zone (HAZ), with the aim of optimizing the heat input and evaluating the mechanical behavior of welded joints. By developing a thermal model of RFW for dissimilar metals [15], characteristics for temperature profile estimation are generated. Furthermore, RFW has been employed for mild steel [35-41], using a FEM to assess the thermal profile and stress propagation. Researchers observed the impact of a correlation between the rise in welding velocity, friction duration, and the elevation in temperature generated by the friction between the two materials. Authors in [16 ,42] developed another numerical model of RFW using a thermomechanical-metallurgical model with FE simulation. The results validated the hypothesis that RFW provides a cost-effective joining process with high-quality welded joints due to the intensive plastic flow within the HAZ [17, 43]. It is essential to recognize the inherent limitations of the RFW process. For instance, RFW is not applicable to welding plate joints due to the lack of uniform thickness in the HAZ resulting from the non-uniform propagation of heat during the welding process [44-45]. There are several advantages to the application of RFW processes, including the ability to be used in a variety of settings. One limitation of RFW is that it is not typically compatible with welding dissimilar materials, which is a challenge that other joining methods do not face. The implementation of high-volume production can significantly enhance design flexibility and suitability for a range of single prototype quantities [25, 38]. This research presents an FEM and experimental validation of the thermomechanical analysis of dissimilar joints of S275 and 316L austenitic stainless steels using RFW. The study employed an FE simulation model, with the design process conducted in SolidWorks. The experimental procedure entailed the combination of thermal cycle measurements with tensile tests, with the objective of evaluating the tensile force, ultimate yield strength, and elongation of the welded joints. Energy Dispersive Scanning (EDS) electron microscopy was employed to examine the microstructure of the HAZ of both base materials, thereby facilitating an investigation of the microstructural alterations in the coarse-grained HAZ.

II. MATERIALS AND METHODS

The software used for the definition of the sample's geometry was SolidWorks 2020. The FE model was generated using the ANSYS software, version 19.2. The following represents a general evaluation of heat propagation in and around the welded joint, which can be written as [9, 16]:

$$\rho Cp\left[\frac{\partial T}{\partial t}+u\frac{\partial T}{\partial X}+v\frac{\partial T}{\partial y}+w\frac{\partial T}{\partial z}\right]=\frac{\partial}{\partial x}\left(k\frac{\partial T}{\partial x}\right)+\frac{\partial}{\partial y}\left(k\frac{\partial T}{\partial y}\right)+\frac{\partial}{\partial z}\left(k\frac{\partial T}{\partial z}\right)+ST \quad (1)$$

where ρ is the density of the material, Cp is the specific heat, and k is the thermal conductivity. The parameters x, y, and z represent different thermal directions (mm). By taking into account all the parameters, it can be reduced to [9, 36]:

$$\rho C_p\frac{\partial T}{\partial t}=\frac{\partial}{\partial x_t}\left[k\frac{\partial T}{\partial x_t}\right]+\rho C_p u\frac{\partial T}{\partial x_1}+\dot{S} \quad (2)$$

where $\dot{S}$ is the volumetric heat source term (W/m^3) rising during rotary friction. The section on the right side in (2) shows the convective aspect of the equation system. The velocity at the side, u, is a factor in the temperature gradient that occurs during RFW. In order to integrate the mechanical, thermal, and metallurgical fields, it is essential to ascertain the interrelationships between them. The interrelated thermomechanical-metallurgical relationship, can be defined as [9]:

$$d\varepsilon_{ij}^{total}=d\varepsilon_{ij}^{el}+d\varepsilon_{ij}^{pl}+d\varepsilon_{ij}^{th}+d\varepsilon_{ij}^{tr}+d\varepsilon_{ij}^{tp} \quad (3)$$

where $d\varepsilon_{ij}^{el}$ is the elastic strain increment, $d\varepsilon_{ij}^{pl}$ is the plastic strain increment, and both the elastic and plastic strains are part of the mechanical fields of analysis. The thermal strain increment is represented by $d\varepsilon_{ij}^{th}$, and the metallurgical field is represented by $d\varepsilon_{ij}^{tr}$, which is the transformation-related strain increment and $d\varepsilon_{ij}^{tp}$ transformation plasticity strain increment. The welding method using RFW needs to consider many factors, such as the rotational speed:

$$\omega = 2\,\pi n \quad (4)$$

where n is the tour number (tr/min). It is important to know the increment friction work ($dW_{FR(i)}$) and dissipation coefficient (β_{FR}) that were used, show the relationship among the contact

surface, the rotation center (r_i), the current frictional shear stress ($\tau_{R(i)}$), the increment time, and the rotational time:

$$dq_{FR(i)} = \beta_{FR}.dW_{FR(i)} \quad (5)$$

$$dq_{FR(i)} = \beta_{FR}.\tau_{R(i)}.\omega.r_i.dt \quad (6)$$

Transient thermal and static structural analyses were completed using ANSYS Workbench software. The objective was to assess the RFW of dissimilar S275 and 316L steels. An FEM of a weld specimen with dimensions of 150 mm in length and a diameter of 7 mm was used. In RFW, two materials (S275 and 316L) are employed, resulting in the generation of 8,147 and 3,030 nodes and elements, respectively. Equation (1) can be solved numerically with the aid of appropriate software in order to evaluate a number of key mechanical properties, including thermal profile, stress distribution, tensile force, ultimate yield stress, and elongation percentage. The experimental procedure was designed with consideration of various parameters, including the rotational speed (welding speed) of the chuck (*w*), feed speed, and weld time. The rotational speed (*V*) varied between 800 rev/min and 2,000 rev/min, while the feed rate was maintained at 63 mm/min. Four distinct samples of each material, with identical diameter (7 mm) and length were meticulously prepared. The variables of friction pressure (*P*) and welding time step (*t*) were varied in accordance with the parameters of rotational speed, feed speed, and time, as presented in Table I. Table II shows the chemical composition of the base material, while Table III outlines the mechanical properties of both materials. A pyrometer was used to measure the thermal cycle. The data were recorded and analyzed using LabView software.

TABLE I. WELD PARAMETERS FOR THE SIMULATION PROCESS

RFW parameter	Number of samples simulated			
	01	02	03	04
Welding speed, *w*	800	1,000	1,600	2,000
Feed speed, *V*	63	63	63	63
Friction pressure, *P*	1.4	1.6	1.8	2.1
Time, *t*	40	40	40	40

TABLE II. CHEMICAL COMPOSITION OF 316L AND S275 STEELS

	C	Si	Mn	Cu	Cr	Ni	Mo	N	P	S
316L	0.018	0.45	0.98	-	17.1	10.0	2.04	0.036	0.038	0.001
S275	0.18	-	1.14	0.56	-	-	-	0.01	0.03	0.035

TABLE III. MECHANICAL AND THERMAL PROPERTIES OF BOTH MATERIALS (S275 AND 316L)

	S275	316L
Yield strength (MPa)	400	317
Tensile strength (MPa)	560	603
Compression strength in *x* (MPa)	34	65
Elongation (%)	18	56
Hardness (HV5)	140	182
Thermal conductivity (W/m^0K)	30	15
Density (kg/m^3)	7,820	7,980

The methodology employed for the FE simulation of RFW, in conjunction with the experimental procedure, is shown in Figure 1. The flowchart presents the commencement and conclusion of the numerical and experimental procedures, as well as the application of a varying speed (*V*) throughout the experimental procedure. RFW of dissimilar AISI 316L stainless steel and general-purpose steel S235 was perfomed on a universal milling machine (Alcera DASES 7874 type 807 horizontal position) equipped with a divider mounted on its table. The tensile test was performed using a hydraulic tensile testing machine, EWTGUWP310 (Ref. 020.31000), which comprises a traction apparatus equipped with two jaws for the grasping of round and flat tensile specimens, a console for the control of the test via its hydraulic control system and the collection of data obtained from the load and displacement sensors. The console is linked to a computer on which the WP 310 data acquisition and processing software is installed for the reception and processing of the collected data. The machine has a maximum load capacity of 50 kN, a maximum pressure of 175 bars, a travel speed range of 2 mm/min to 425 mm/min, and a maximum piston stroke of 150 mm. The tests were conducted in accordance with the standards set forth in EN ISO 6892-1:2016 [37]. Corner jaws with striated bits were used for the round specimens, with a test speed of 2 mm/min. Following the adjustment of the requisite distance between the jaws to position the specimen and the mounting of the appropriate bits in the jaws, the machine, specifically the console and the computer, was initiated. The specimen was then mounted in the jaws of the traction device, as shown in Figure 1.

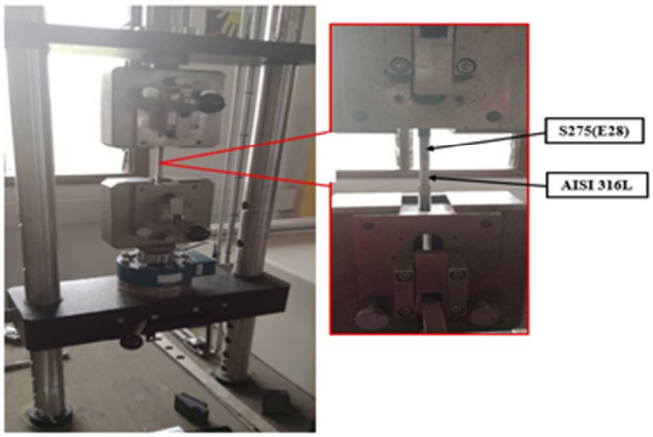

Fig. 1. The hydraulic tensile testing machine: EWTGUWP310.

III. RESULTS AND DISCUSSION

The values obtained from the FE simulation model and the results of the experimental procedure conducted on dissimilar S275-316L are presented in Figure 2. The results of the FE simulation model and the experimental method exhibit a high degree of correlation with regard to the evaluation of the thermal distribution in the HAZ. Figure 2 presents the simulation and experimental results for the temperature distribution from the melting zone to the base material in S275 steel, along with the numerical and experimental results of the thermal distribution. With a welding speed of 800 rev/min (S1), the maximum temperature reached was 1,200 °C in the experimental procedure and 1,149 °C in the FE-simulation model. The lowest temperature recorded during the cooling phase was approximately 95 °C for S275 steel and 320 °C for 316L steel. The higher cooling temperature observed for the

316L steel can be attributed to its lower thermal conductivity compared to the S275 steel. An increase in the welding speed to 1,000 rev/min resulted in an elevated melting temperature (1,300 °C). An increase in the cooling temperature was observed on the 316L side, while minimal change was noted on the S275 side. The same observations were made when the welding speed was 1600 rev/min. The measured melting temperature was 1350 °C, which was in close agreement with the calculated value. The cooling temperature exhibited an increase of 450 °C for the 316L side and 178 °C for the S275 side. An increase in the welding speed (2,000 rev/min) resulted in a notable rise in the melting temperature (1,400 °C) compared to the other welding speed values employed. An increase in the cooling temperature was observed for both sides, with values of 190 °C and 600 °C for S275 and 316L, respectively. The discrepancy between the FE-numerical model and the experimental temperature profile for the peak temperature calculation was determined to be 2.78%.

The longitudinal sections of each sample welded at varying rotational speeds are presented in Figure 3, in which the formation of flash is indicated by a red circle. It is observed that the cross-section of the welded sample at a speed of 800 rpm exhibits an irregular joint plane due to incomplete expulsion of impurities. Additionally, the weld joint plane does not fully encompass the specimen section, likely due to insufficient volume of the creating flash. As can be observed in Figure 3, the weld plane is more regulated in the sample welded at 1,000 rpm. There is a notable reduction in impurities, and the weld joint plane demonstrates a more comprehensive coverage of the section. The impurities are expelled entirely into the weld joint of the specimen section, which is then completely covered by the weld joint at 1,600 rpm and 2,000 rpm.

Figure 4 shows the stress distribution for a welding speed of 800 rev/min. The normal stress distribution exhibits a maximum normal stress value of 12.362 MPa and is focused along the x-axis. The equivalent (von Mises) stress has a maximum value of 1,438.9 MPa, which is observed in the HAZ of the sample. The elastic deformation and the methodology employed to quantify it, are shown in Figure 4. The findings were validated by [31-32], particularly in the context of 316L steel, although the identical welding procedure was not used.

The results of the FE simulation and experimental analysis of the tensile strength and ultimate tensile strength function of the elongation are presented in Figure 5. Upon application of a welding speed of 800 tr/min, the results demonstrate a tensile force value of 2.5 kN (depicted in blue) as predicted by the FE simulation, and an experimental value of 3.5 kN. The ultimate yield strengths observed were 65 MPa and 90 MPa for the FE simulation model and experimental results, respectively. A notable discrepancy exists between the values obtained from the simulation model and those derived from the experimental procedure. Upon increasing the welding speed to 1,000 tr/min, the elongation exhibited a notable increase, reaching 4.5 mm. The tensile strength values were 3.8 kN and 4 kN, respectively, for the simulation analysis and the experimental procedure.

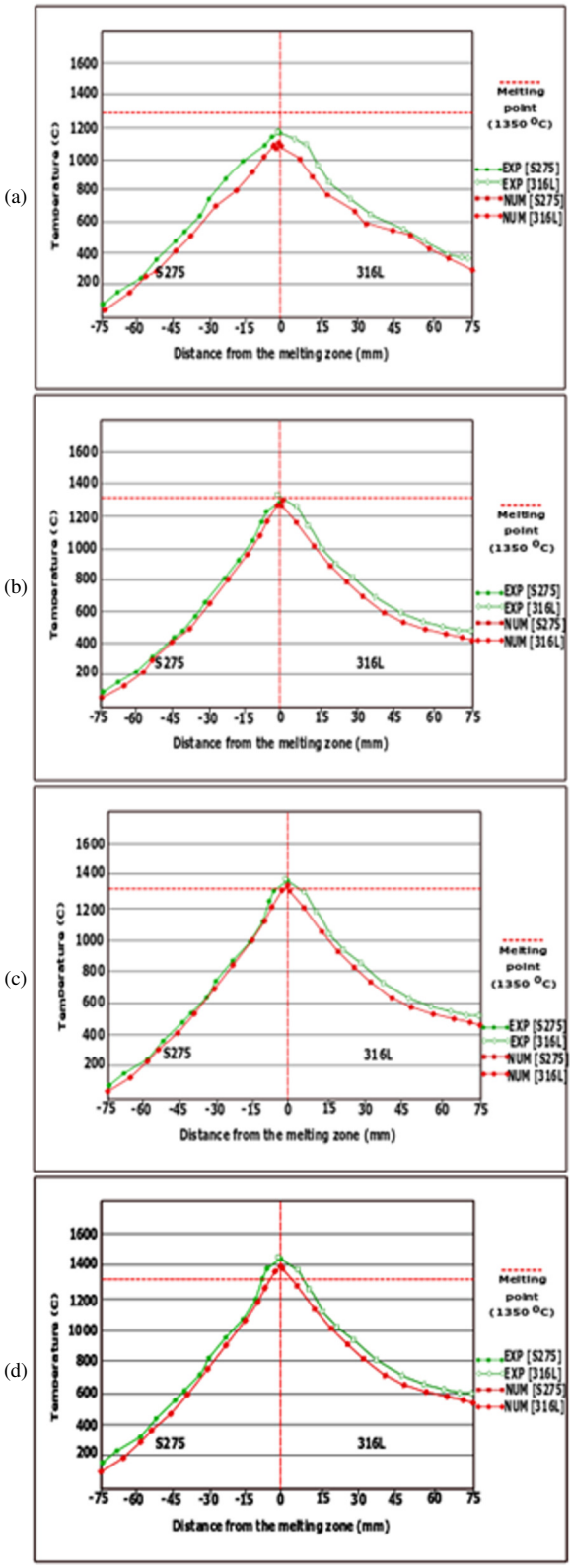

Fig. 2. FE-simulation model and experimental results of the thermal profile of dissimilar S275/316L at (a) a welding speed of 800 rev/min, (b) a welding speed of 1000 rev/min, (c) a welding speed of 1600 rev/min, and (d) 2000 rev/min.

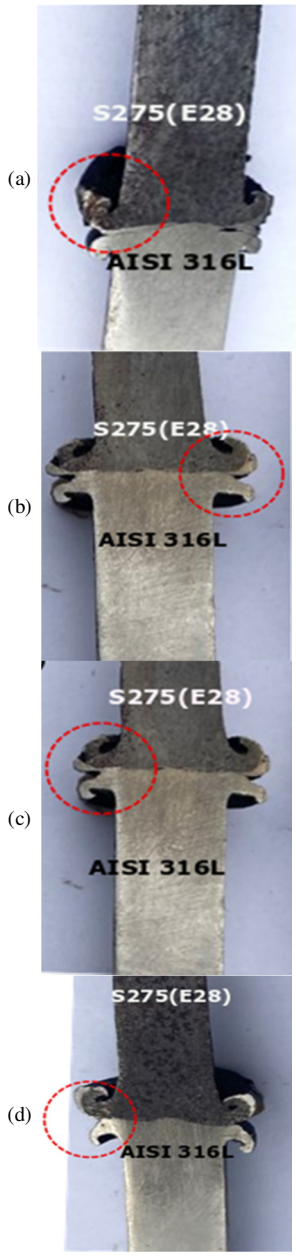

Fig. 3. Longitudinal sections of each sample welded at rotational speeds of (a) 800 rev/min, (b) 1000 rev/min, (c) 1600 rev/min, and (d) 2000 rev/min.

The ultimate yield strengths were found to be 116 MPa and 120 MPa, respectively, for the simulation analysis and an experimental test. The tensile force distribution and yield strength function of the welded joint of RFW, as a function of elongation, is also shown in Figure 5. The welding speed applied was 1,600 tr/min, resulting in increases of 7 kN and 8 kN for the FE simulation and experimental procedures, respectively. The ultimate yield strengths were found to be 200 MPa and 195 MPa, respectively, for the numerical analysis and experimental test. An increase in the welding speed results in an increase in both the tensile force and the ultimate yield. A welding speed of 2,000 tr/min is thus recommended.

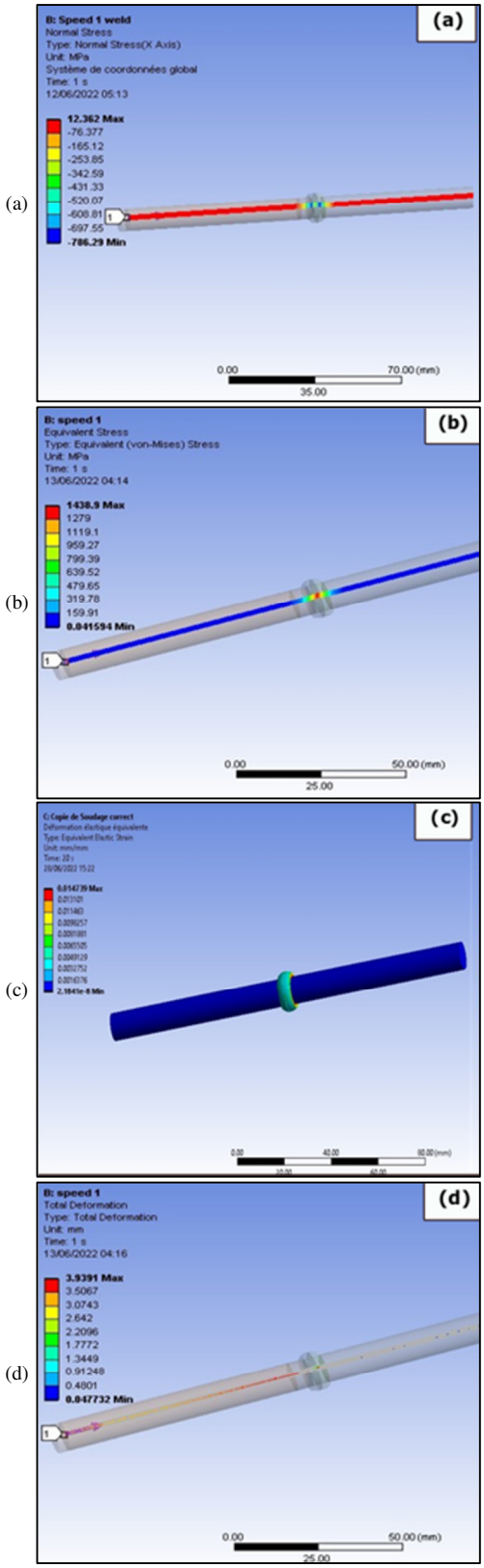

Fig. 4. Stress distribution using a welding speed of 800 rev/min; (a) normal stress distribution, (b) equivalent stress, (c) elastic deformation, and (d) elongation measurements.

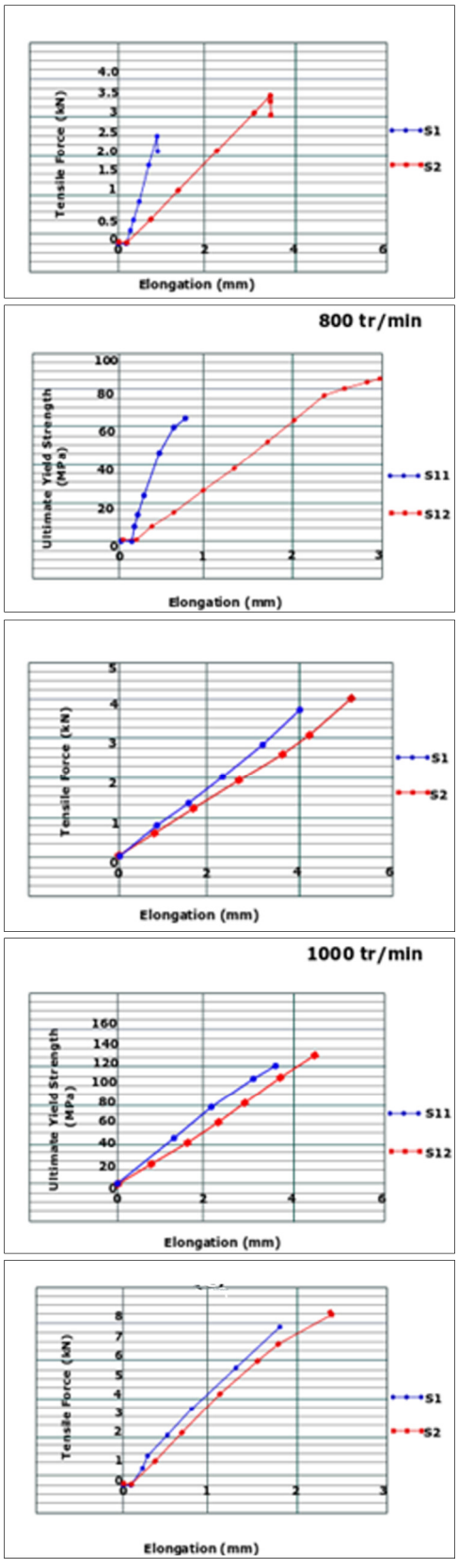

Fig. 5. FE-simulation and experimental analysis of tensile strength and the ultimate tensile strength function of the elongation; (a) welding speed of 800 rev/min, (b) welding speed of 1000 rev/min, (c) welding speed of 1600 rev/min, and (d) 2000 rev/min.

The same behavior was observed for this sample, as shown in Figure 5. The results demonstrate an increase in tensile strength of up to 15 kN and an increase in ultimate yield strength of 400 MPa for both analysis processes. The discrepancy in the tensile test outcomes can be attributed to the specific parameters employed in the friction welding process, namely the welding speed, feed speed, and friction pressure. Furthermore, the use of dissimilar materials has an impact on materials with lower tensile and yield strength. There is a discrepancy between the experimental and simulation results following tensile analysis. Upon examination of both methods (experimental and numerical), it is determined that the welded joint error calculation of the tensile force at this juncture is 12%. The error in the ultimate yield strength for the disparate samples calculated is found to be less than the tensile force's (6%). To substantiate the mechanical properties (strength), an Energy Dispersive Spectroscopy (EDS) analysis was conducted on the Coarse Grain Heat Affected Zone (CGHAZ), which exhibited a more pronounced response to the elevated temperature at a speed of 2000 rev/min. Figure 6 (S275, fusion line) presents that a minimal quantity of carbide is produced as

a consequence of the elevated peak temperature at the melting point. The microstructural state is formed in the fusion line, which is then followed by carbide dissolution and precipitation and an increase in the carbon content is obvious within the microstructure.

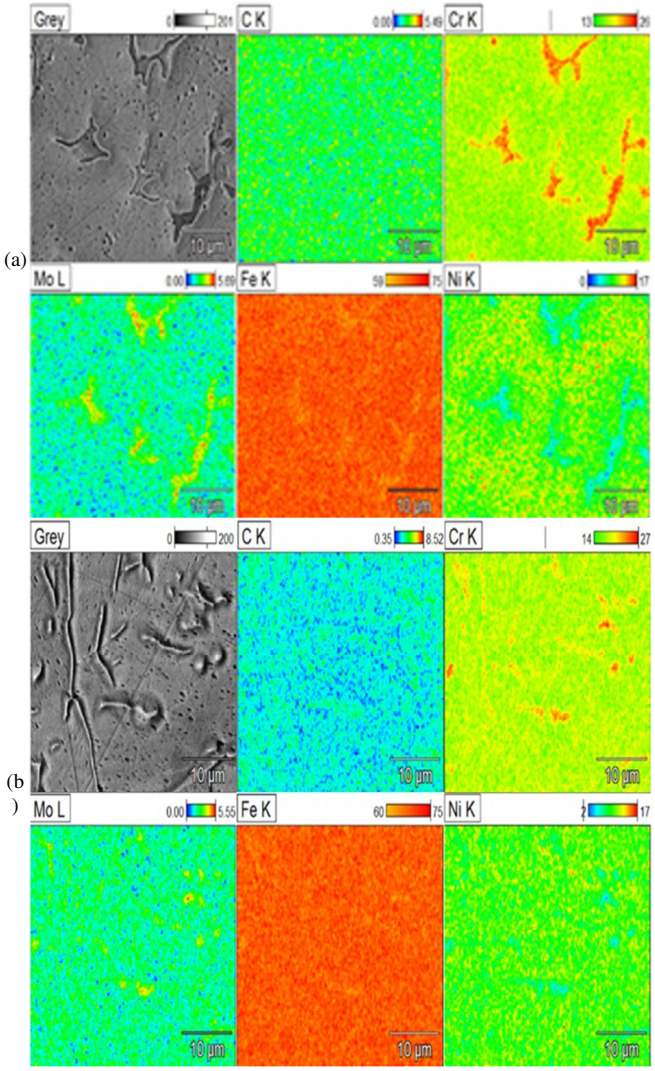

Fig. 6. SEM–EDS analysis and alloy element composition in the CGHAZ of dissimilar weld joints: (a) 316L and (b) S275.

The elevated carbon content observed in the fusion zone can be attributed to the higher peak temperature. The formation of traces of nickel, molybdenum, and chrome in the microstructure (fusion line) was also observed. This can be explained by the fact that a fusion has occurred between the two materials. The base material does not contain any nickel or chrome in its microstructure. It is imperative that an additional test be developed to ascertain whether crack propagation occurs in welded joints. Figure 6 presents the formation of carbides. This was a consequence of the elevated welding speed (2000 rev/min) and friction pressure (2.1 MPa), which resulted in an increased temperature in the fusion line. The microstructure exhibited increases in chromium and nickel of 1.2% and 1.01%, respectively, in comparison to the base metal. The same increase in the amount of C, Cr, and Ni has been corroborated in numerous instances [31, 32, 38, 39]. There are multiple ways to justify the increase in the amount of C. It is recommended to conduct an EDS analysis on a well-prepared specimen to gain further insight. Authors in [40] attempted to reduce the C content by optimizing the welding parameters, which resulted in an improved yield strength of the welded joints.

IV. CONCLUSIONS

The present study employed Finite Element (FE) simulations and experimental analyses to investigate the thermomechanical properties of dissimilar welded S275 and 316L austenitic stainless steels using Rotary Friction Welding (RFW) processes. A FE simulation model was constructed using 3D nonlinear (ANSYS 19.1) software to determine the temperature profile, tensile force, ultimate yield strength, deformation in the Heat-Affected Zone (HAZ), and microstructural constituents in the fusion zone of the welded joints. The same analysis was conducted using experimental methods. To conduct the RFW process, four welding speeds were employed (800 rev/min, 1000 rev/min, 1600 rev/min, and 2000 rev/min). The following findings can be reported:

- It is crucial to acknowledge the impact of welding speed (a pivotal concept) on the thermal profile of the welded specimen when employing the RFW technique. An increase in the welding speed has an impact on the thermal, mechanical, and metallurgical analysis of RFW.
- The results demonstrate a high degree of concordance between the FE simulation and experimental procedures with regard to the thermal profile and ultimate yield strength, particularly when a welding speed of 2000 rev/min is employed.
- At a welding speed of 800 rev/min, the results demonstrated a lack of fusion within both materials, which was attributed to a hydrogen crack in the welded joint. The welded joint did not extend across the entire specimen section due to the insufficient volume of the flash created during the welding process.
- A higher temperature was recorded and calculated (1,450 ^{o}C) when the welding speed was 2000 rev/min, and failure was observed on the S275 side when the tensile test was applied.
- At a welding speed of 2000 rev/min, the tensile force, ultimate yield strength, and elongation were found to be 14.025 kN, 364.44 MPa, and 14%, respectively.
- The microstructure of the fusion zone exhibited an increase in chromium and nickel content, with values of 1.2% and 1.01%, respectively, in comparison to the base metal of 316L stainless steel. Additionally, an increase in carbon content was observed.

This study presents a reasonable correlation between the temperature profile predicted by the FE-simulation model and the experimental data of RFW, in which the welding speed varies during the welding process. The model allows for the

validation of the relationships between the welding process, temperature profile, and mechanical properties in the HAZ. The results obtained can be employed to predict the microstructural constituents in the HAZ and to evaluate the composition of the allowable elements in samples subjected to welding.

REFERENCES

[1] P. Kah, M. Shrestha, and J. Martikainen, "Trends in Joining Dissimilar Metals by Welding," *Applied Mechanics and Materials*, vol. 440, pp. 269–276, 2014, https://doi.org/10.4028/www.scientific.net/AMM.440.269.

[2] "Welding-dissimilar –metals," Australian Stainless Steel Development Association, Brisbanqld, Australia, Technical, 2022.

[3] S. S. Murugan, P. Sathiya, and A. N. Haq, "Rotary Friction Welding and Dissimilar Metal Joining of Aluminium and Stainless Steel Alloys," *Annals of Dunarea de Jos University of Galati, Welding Equipment and Technology*, vol. 32, pp. 85–92, Dec. 2021, https://doi.org/10.35219/awet.2021.11.

[4] L. Bastos *et al.*, "Transmission laser welding of thermoplastics: Influence of welding parameters and rib dimensions on the strength of welded joints," *Journal of Advanced Joining Processes*, vol. 8, Dec. 2023, Art. no. 100173, https://doi.org/10.1016/j.jajp.2023.100173.

[5] S. Kralj, "Welding and Allied Processes," in *Welding Engineering and Technology*, vol. 1, Zagreb, Croatia: Encyclopedia of Life Support Systems, 2024.

[6] S. Kou, *Welding Metallurgy*, 2nd ed. Hoboken, NJ, USA: Wiley, 2002.

[7] E. Akca and A. Gürsel, "Solid State Welding and Application in Aeronautical Industry," *Periodicals of Engineering and Natural Sciences (PEN)*, vol. 4, no. 1, pp. 1–8, Feb. 2016, https://doi.org/10.21533/pen.v4i1.46.

[8] H. Oikawa, S. Ohmiya, T. Yoshimura, and T. Saitoh, "Resistance spot welding of steel and aluminium sheet using insert metal sheet," *Science and Technology of Welding and Joining*, vol. 4, no. 2, pp. 80–88, Apr. 1999, https://doi.org/10.1179/136217199101537608.

[9] S. S. Bhate and S. Bhatwadekar, "A literature review of research on rotary friction welding," *International Journal of Innovative Technology and Research*, vol. 4, no. 1, pp. 2601–2604, Jan. 2016.

[10] N. Shete and S. U. Deokar, "A review paper on rotary friction welding, International conference on ideas," *International Conference on Ideas, Impact and Innovation in Mechanical Engineering*, vol. 5, no. 6, pp. 1557–1560, Jun. 2017.

[11] A. B. Dawood, S. I. Butt, G. Hussain, M. A. Siddiqui, A. Maqsood, and F. Zhang, "Thermal Model of Rotary Friction Welding for Similar and Dissimilar Metals," *Metals*, vol. 7, no. 6, Jun. 2017, Art. no. 224, https://doi.org/10.3390/met7060224.

[12] M. Maalekian, "Thermal Modeling of Friction Welding," *ISIJ International*, vol. 48, no. 10, pp. 1429–1433, 2008, https://doi.org/10.2355/isijinternational.48.1429.

[13] Y. Yohanes, R. Abdurrahman, and A. Ridwan, "Finite element study on rotary friction welding process for mild steel," *IOP Conference Series: Materials Science and Engineering*, vol. 620, no. 1, Sep. 2019, Art. no. 012111, https://doi.org/10.1088/1757-899X/620/1/012111.

[14] M. A. Tashkandi, "Finite element modeling of continuous drive friction welding of Al6061 alloy," *Materials Science-Poland*, vol. 39, no. 1, pp. 1–14, May 2021, https://doi.org/10.2478/msp-2021-0001.

[15] X. Sun, E. V. Stephens, M. A. Khaleel, H. Shao, and M. Kimchi, "Resistance Spot Welding of Aluminum Alloy to Steel with Transition Material - From Process to Performance - Part I: Experimental Study," *Welding Journal*, vol. 83, no. 6, Jun. 2004.

[16] B. Behrens, A. Chugreev, C. Kock, K. Brunotte, T. Matthias, and H. Wester, "FE-simulation of rotary friction welding process considering thermo- mechanical-metallurgical coupling," *Engineering, Materials Science*, 2020.

[17] A. U. Rehman, N. K. Babu, M. K. Talari, Y. S. Usmani, and H. Al-Khalefah, "Microstructure and Mechanical Property Correlation Between Rotary Friction Welded Nitinol–Nitinol Joints," *Frontiers in Materials*, vol. 8, Nov. 2021, https://doi.org/10.3389/fmats.2021.726383.

[18] "Types Of Welding – Classification of welding processes | Welding & NDT," Sep. 04, 2017. https://www.weldingandndt.com/types-of-welding-classification-of-welding-processes.

[19] M. R. Nezamdost, M. R. N. Esfahani, S. H. Hashemi, and S. A. Mirbozorgi, "Investigation of temperature and residual stresses field of submerged arc welding by finite element method and experiments," *The International Journal of Advanced Manufacturing Technology*, vol. 87, no. 1, pp. 615–624, Oct. 2016, https://doi.org/10.1007/s00170-016-8509-4.

[20] W. Li and V. Patel, "Solid State Welding for Fabricating Metallic Parts and Structures," in *Encyclopedia of Materials: Metals and Alloys*, vol. 4, F. G. Caballero, Ed. Oxford, UK: Elsevier, 2022, pp. 246–259.

[21] KUKA, "Friction Welding, " *KUKA Deutschland GmbH, Zugspitzstraße* 140, 86165 Augsburg, Germany. https://www.twi-global.com/technical-knowledge/faqs/faq-what-is-friction-welding, Germany, 2022.

[22] R. Siedlec and C. Strąk, "Rotary friction welding of Al/Al2O3 Composites with Aluminium Alloys," *Welding Technology Review*, vol. 92, no. 6, pp. 23–34, Aug. 2020, https://doi.org/10.26628/wtr.v92i6.1124.

[23] H. T. My Nu, T. T. Le, L. P. Minh, and N. H. Loc, "A Study on Rotary Friction Welding of Titanium Alloy (Ti6Al4V),"*Advances in Materials Science and Engineering*, vol. 2019, no. 1, 2019, Art. no. 4728213, https://doi.org/10.1155/2019/4728213.

[24] K. Mucic, J. Lopera, F. Fuchs, and N. Enzinger, "Linear friction welding of high strength chains: modelling and validation: International Seminar Numerical Analysis of Weldability," in *International Seminar Numerical Analysis of Weldability*, Seggau, Austria, 2012, vol. 10.

[25] *Rotary Friction Welding, American Friction welding*. WI, USA: American Welding Society, 2021.

[26] R. G. Rizvanov, D. S. Mulikov, D. V. Karetnikov, A. M. Fairushin, and A. S. Tokarev, "Evaluation of the Possibility of Obtaining Tube-to-Tube Sheet Welded Joints of 15Cr5Mo Steel by Alternative Technological Process," *IOP Conference Series: Materials Science and Engineering*, vol. 317, no. 1, Mar. 2018, Art. no. 012077, https://doi.org/10.1088/1757-899X/317/1/012077.

[27] A. Afriansyah and A. Arifin, "Dissimilar metal welding using Shielded metal arc welding: A Review," *Technology Reports of Kansai University*, vol. 62, pp. 1935–1948, Apr. 2020.

[28] M. Pietrzak, K. Wałęsa, J. Górecki, and M. Berdychowski, "Analysis of the friction (spin) welding – preliminary study," *MATEC Web of Conferences*, vol. 254, 2019, Art.. no. 02036, https://doi.org/10.1051/matecconf/201925402036.

[29] S. V. Alagarsamy, M. Ravichandran, M. Arunkumar, and C. B. Thivi, "Microstructure and Mechanical Characterization of Friction Welding Process - A Review," *International Journal of Engineering Research & Technology*, vol. 7, no. 2, Apr. 2019, https://doi.org/10.17577/IJERTCONV7IS02020.

[30] A. K. Nasution, P. Nawangsari, A. Junaidi, and H. Hermawan, "Friction welding of AZ31-SS316L for partially-degradable orthopaedic pins," *IOP Conference Series: Materials Science and Engineering*, vol. 532, Jun. 2019, Art. no. 012014, https://doi.org/10.1088/1757-899X/532/1/012014.

[31] E. P. Alves, R. C. Toledo, F. Piorino Neto, F. G. Botter, and C. Ying An, "Experimental Thermal Analysis in Rotary Friction Welding of Dissimilar Materials," *Journal of Aerospace Technology and Management*, vol. 11, Sep. 2019, Art. no. e4019, https://doi.org/10.5028/jatm.v11.1068.

[32] N. S. Kalsi and V. S. Sharma, "A statistical analysis of rotary friction welding of steel with varying carbon in workpieces," *The International Journal of Advanced Manufacturing Technology*, vol. 57, no. 9, pp. 957–967, Dec. 2011, https://doi.org/10.1007/s00170-011-3361-z.

[33] M. Ramdani, M. Benachour, and M. Rahou, "The Effects of Resistance Spot Welding Parameters on the Mechanical Behavior of Stainless Steel," *Engineering, Technology & Applied Science Research*, vol. 13, no. 2, pp. 10501–10504, Apr. 2023, https://doi.org/10.48084/etasr.5019.

[34] F. N. Bayock, P. Kah, M. Kibong, and S. Timba, "Thermal induced residual stress and microstructural constituents of dissimilar S690QT high-strength steels and 316L austenitic stainless steel weld joints," *Materials Research Express*, vol. 8, no. 7, Jul. 2021, Art. no. 076519, https://doi.org/10.1088/2053-1591/ac15d8.

[35] F. Ternane, M. Benachour, F. Sebaa, and N. Benachour, "Regression Modeling and Process Analysis of Resistance Spot Welding on Dissimilar Steel Sheets," *Engineering, Technology & Applied Science Research*, vol. 12, no. 4, pp. 8896–8900, Aug. 2022, https://doi.org/10.48084/etasr.5059.

[36] F. N. Bayock, P. Kah, P. Layus, and V. Karkhin, "Numerical and Experimental Investigation of the Heat Input Effect on the Mechanical Properties and Microstructure of Dissimilar Weld Joints of 690-MPa QT and TMCP Steel," *Metals*, vol. 9, no. 3, Mar. 2019, Art. no. 355, https://doi.org/10.3390/met9030355.

[37] International standard test methods for tensile testing of metallic materials, ISO 6892-1. Geneva, Switzerland: International Standard Organization, 2016.

[38] F. N. Bayock, P. Kah, K. M. Tony, F. N. Bayock, P. Kah, and K. M. Tony, "Heat input effects on mechanical constraints and microstructural constituents of MAG and laser 316L austenitic stainless-steel welded joints," *AIMS Materials Science*, vol. 9, no. 2, pp. 236–254, 2022, https://doi.org/10.3934/matersci.2022014.

[39] C.-C. Kuo, A. Farooqui, N. Gurumurthy, and S.-H. Huang, "Effects of rotational speed on the microstructure and mechanical properties of continuous drive friction welding of dissimilar composite polymer rods," *The International Journal of Advanced Manufacturing Technology*, vol. 134, no. 5, pp. 2547–2561, Sep. 2024, https://doi.org/10.1007/s00170-024-14261-9.

[40] A. A. Mattie, S. Y. Ezdeen, and G. I. Khidhir, "Optimization of parameters in rotary friction welding process of dissimilar austenitic and ferritic stainless steel using finite element analysis," *Advances in Mechanical Engineering*, vol. 15, no. 7, Jul. 2023, Art. no. 16878132231186015, https://doi.org/10.1177/16878132231186015.

[41] P. Prasath and R. Prabu, "Analysis of Dissimilar Metal Welding of 1020 Mild Steel and 304 Stainless Steel," *International Journal for Scientific Research and Development*, vol. 7, no. 12, pp. 126–128, Mar. 2020.

[42] H. Aberbache, A. Mathieu, R. Bolot, L. Bleurvacq, A. Corolleur, and F. Laurent, "Experimental analysis and numerical simulation of Laser welding of thin austenitic stainless-steel sheets using two models: Bilinear isotropic strain hardening model and Johnson–Cook model," *Journal of Advanced Joining Processes*, vol. 9, Jun. 2024, Art. no. 100198, https://doi.org/10.1016/j.jajp.2024.100198.

[43] A. Banerjee, L. da Silva, and S. Rahimi, "Finite element modelling of transient behaviours and microstructural evolution during dissimilar rotary friction welding of 316 austenitic stainless steel to A516 ferritic steel," *Journal of Advanced Joining Processes*, vol. 8, Nov. 2023, Art. no. 100167, https://doi.org/10.1016/j.jajp.2023.100167.

[44] C.-C. Kuo, N. Gurumurthy, H.-W. Chen, and S.-H. Huang, "Analysis of temperature history, fatigue behavior and surface hardness in rotary friction welded dissimilar polymer rods with variable rotational speeds," *Journal of Advanced Joining Processes*, vol. 9, Jun. 2024, Art. no. 100211, https://doi.org/10.1016/j.jajp.2024.100211.

[45] J. Zhang, M. H. R. Dehkordi, M. J. Kholoud, H. Azimy, and S. Daneshmand, "Experimental and numerical study of melt flow, temperature behavior and heat transfer mechanisms during the dissimilar laser welding process," *Optics & Laser Technology*, vol. 180, Jan. 2025, Art. no. 111521, https://doi.org/10.1016/j.optlastec.2024.111521.